



# Cryo-EM structure of a tetrameric cyanobacterial photosystem I complex reveals novel subunit interactions



Dmitry A. Semchonok<sup>a</sup>, Meng Li<sup>b,c</sup>, Barry D. Bruce<sup>b,c,d,e,\*</sup>, Gert T. Oostergetel<sup>a</sup>, Egbert J. Boekema<sup>a,\*\*</sup>

<sup>a</sup> Department of Electron Microscopy, Groningen Biomolecular Sciences & Biotechnology Institute, University of Groningen, 9747 AG Groningen, The Netherlands

<sup>b</sup> Department of Biochemistry, Cellular, and Molecular Biology, University of Tennessee, Knoxville, TN 37996, USA

<sup>c</sup> Bredesen Center for Interdisciplinary Research and Graduate Education, University of Tennessee, Knoxville, TN 37996, USA

<sup>d</sup> Department of Microbiology, University of Tennessee, Knoxville, TN 37996, USA

<sup>e</sup> Sustainable Energy and Education Research Center, University of Tennessee, Knoxville, TN 37996, USA

## ARTICLE INFO

### Article history:

Received 19 May 2016

Received in revised form 25 June 2016

Accepted 28 June 2016

Available online 5 July 2016

### Keywords:

Photosystem I

Electron microscopy

Structure

Cyanobacteria

*Chroococcidiopsis*

## ABSTRACT

Photosystem I (PSI) of the thermophilic cyanobacterium *Chroococcidiopsis* sp. TS-821 (TS-821) forms tetramers Li et al. (2014). Two-dimensional maps obtained by single particle electron microscopy (EM) clearly show that the tetramer lacks four-fold symmetry and is actually composed of a dimer of dimers with C2 symmetry. The resolution of these negative stain 2D maps did not permit the placement of most of the small PSI subunits, except for PsaL. Therefore cryo-EM was used for 3D reconstruction of the PSI tetramer complex. A 3D model at ~11.5 Å resolution was obtained and a 2D map within the membrane plane of ~6.1 Å. This data was used to build a model that was compared with the high-resolution structure of the PSI of *Thermosynechococcus elongatus* (*T. elongatus*) at 2.5 Å. This comparison reveals key differences in which subunits are involved in the two different interfaces, interface type 1 within a dimer and interface type 2 between dimers. The type 1 interface in TS-821 is similar to the monomer interface in the trimeric PSI from *T. elongatus*, with interactions between subunits PsaA, -B, -I, -L and M. In type 2 the interaction is only between PsaA, -B and -L. Unlike the trimeric PSI, the central cavity of the complex is not filled with the PsaL-derived helical bundle, but instead seems filled with lipids. The physiological or evolutionary advantage of the tetramer is unknown. However, the presence of both dimers and tetramers in the thylakoid membrane suggest a dynamic equilibrium that shifts towards the tetramers in high light.

© 2016 Elsevier B.V. All rights reserved.

## 1. Introduction

Photosystem I (PSI) is one of the main membrane proteins involved in the primary steps in oxygenic photosynthesis. The protein catalyzes the electron transfer from plastocyanin/cytochrome *c* to ferredoxin/ferredoxin. Electrons are finally used to reduce NADP<sup>+</sup> to NADPH necessary for the reduction of CO<sub>2</sub> in the Calvin cycle. It is a multi-subunit protein, of which the central subunits PsaA and PsaB are by far the largest subunits and harbor most of the chlorophylls and carotenoids of the antenna system. These two subunits are conserved in evolution and are present in all organisms capable of oxygenic photosynthesis, including cyanobacteria, algae and higher plants. One monomeric unit of cyanobacterial PSI consists of 12 different subunits (PsaA–PsaF, PsaI–PsaM and PsaX), to which 127 cofactors are non-covalently bound [2]. During the course of evolution the structure of cyanobacteria and higher plants PSI diverged significantly.

Much of our knowledge about PSI is based on high-resolution structures. A trimer structure of 2.5 Å resolution from the cyanobacterium *Thermosynechococcus elongatus* was obtained by X-ray crystallography in 2001 [3], which was later followed by a plant monomeric PSI structure that could be successively improved [4,5]. From these and previous studies [3,6,7], we know that PSI consists of a reaction center and electron transfer chain surrounded by a pigment antenna array of ~105 Chl *a* [8] held together non-covalently by a protein scaffold [9]. The cyanobacterial PSI trimer has a cloverleaf structure with a diameter of 220 Å and a transmembrane thickness of ~40 Å. However, it has a stromal “hump” that extends above the bilayer by about 50 Å at the stromal surface bringing the maximum thickness to ~90 Å. The stromal hump is formed by subunits PsaC, PsaD and PsaE, which provide the docking site for the electron acceptors ferredoxin or flavodoxin. In the transmembrane region of trimeric PSI, the subunits PsaF, PsaJ, PsaK and PsaX are located at the distal side of the PSI, while PsaL, PsaI and PsaM are located at the interface between the monomers, with PsaL forming the connection domain that structurally and functionally links the monomers [2]. PsaI is a small subunit of PSI containing one transmembrane helix and does not bind chlorophyll. Instead it forms hydrophobic interactions with carotenoid molecules and may further stabilize the trimerization

\* Correspondence to: B.D. Bruce, Bredesen Center for Interdisciplinary Research and Graduate Education, University of Tennessee, Knoxville, TN 37996, USA.

\*\* Corresponding author.

E-mail addresses: [bbruce@utk.edu](mailto:bbruce@utk.edu) (B.D. Bruce), [e.j.boekema@rug.nl](mailto:e.j.boekema@rug.nl) (E.J. Boekema).

between PsaL and PsaM [2]. PsaM contains also only one transmembrane  $\alpha$ -helix. It is the smallest subunit of PSI with a MW of 3.4 kDa. It is located at the monomer/monomer interface, and forms interactions with PsaL and PsaB [10].

The PsaL subunit is known to display important structural differences between photosynthetic eukaryotes (plants/algae) and cyanobacteria. In these eukaryotes, PsaL is exposed on the surface of PSI and is stabilization via interaction with PsaH [11] a protein of subunit of PSI that is absent in cyanobacteria. The presence of PsaH plus the absence of the PsaM subunit somehow prevent trimer formation in plant PSI [9]. In addition to PsaH, plant PSI contains some other peripheral small subunits, including PsaN and PsaG. The last one creates an anchoring point for 4 Lhca antenna pigment-protein complexes (Lhca1-Lhca4) that are absent in cyanobacteria. PsaH, PsaG, PsaN and PsaO are special to eukaryotes and are involved in binding the light harvesting complexes as well [12,13]. In higher plants the peripheral light-harvesting antenna complex I (LHCI) is restricted to four subunits binding in a 1:1 ratio, but in some algae LHCI can consist of nine different proteins [14]. Thus it is clear that the loss of the three fold axis of symmetry in PSI in plants and algae has now provided two opposing faces of PSI (the PsaL/H surface and the PsaF surface) that individually can interact with additional yet distinct peripheral pigment-proteins complexes, LHCI and LHCII. It has also been shown that the placement of PsaH next to PsaL is key for state transitions in plant photosynthesis [15].

Due to the initial characterization of a trimeric PSI complex in cyanobacteria, it has been widely accepted that the trimer is the only multimeric form of PSI found in cyanobacteria [16–19]. Recently, tetrameric forms of PSI association were found, as reported in *Anabaena* sp. PCC 7120 [20,21] and *Chroococcidiopsis* sp. TS-821 [1], hereafter called *Anabaena* and *Chroococcidiopsis*. Initial comparison of the sequences of some small subunits indicated that at least PsaL and PsaI subunits of the tetramer-forming cyanobacteria are different in respect to the trimer-forming species. Thus the trimeric or tetrameric organization could be determined by the set of PsaL and PsaI in the PSI supercomplex [20]. Moreover, the low-resolution EM maps of

*Anabaena* and *Chroococcidiopsis* pointed out that the association of the monomers into the tetramers is clearly different from the trimer association [1,21]. In the case of the trimeric organization of *T. elongatus*, the PsaL subunit of one monomer directly interacts with the PsaL subunits of the other two monomers [3]. In this study we have applied cryo-EM to obtain higher resolution EM structures to get insight in the details of the tetramer and in particular of the subunits responsible for the contacts between the monomers. By combining a 3D cryo-EM structure with the high-resolution structure of the monomer from the trimer [2] we are able to show that the small subunits PsaL and PsaI make different contacts within the two interfaces of the tetramer. We find that *Chroococcidiopsis* is able to assemble small amounts of trimers, in addition to the tetramers. We also observe that the ratio of tetramer to trimer is variable and responsive to light levels. This change is discussed in how cyanobacteria might regulate their oligomeric state of PSI, as a primitive form of photo-adaptation and a possible prerequisite for further evolutionary changes.

## 2. Materials & methods

### 2.1. PSI tetramer isolation

Isolation of *Chroococcidiopsis* sp. TS-821 PSI tetramers were performed as described in the previous chapter and paper [1]. They were stored frozen in a buffer that contained 50 mM MES (2-(*N*-morpholino)ethanesulfonic acid), pH 6.5, 10 mM MgCl<sub>2</sub> and 5 mM CaCl<sub>2</sub> at a concentration of 0.32 mg/ml Chl and 0.01%  $\beta$ -dodecyl maltoside ( $\beta$ -DDM, Glycon Biochemicals, Luckenwalde, Germany).

### 2.2. High light stress response analyses

TS-821 dense liquid culture (2 l) under continuous low light (LL, 40  $\mu$ E/m<sup>2</sup>/s) was divided into two cultures and then supplemented with fresh BG-11 media for an additional two-day continuous growth under different light intensities before harvesting. For low light

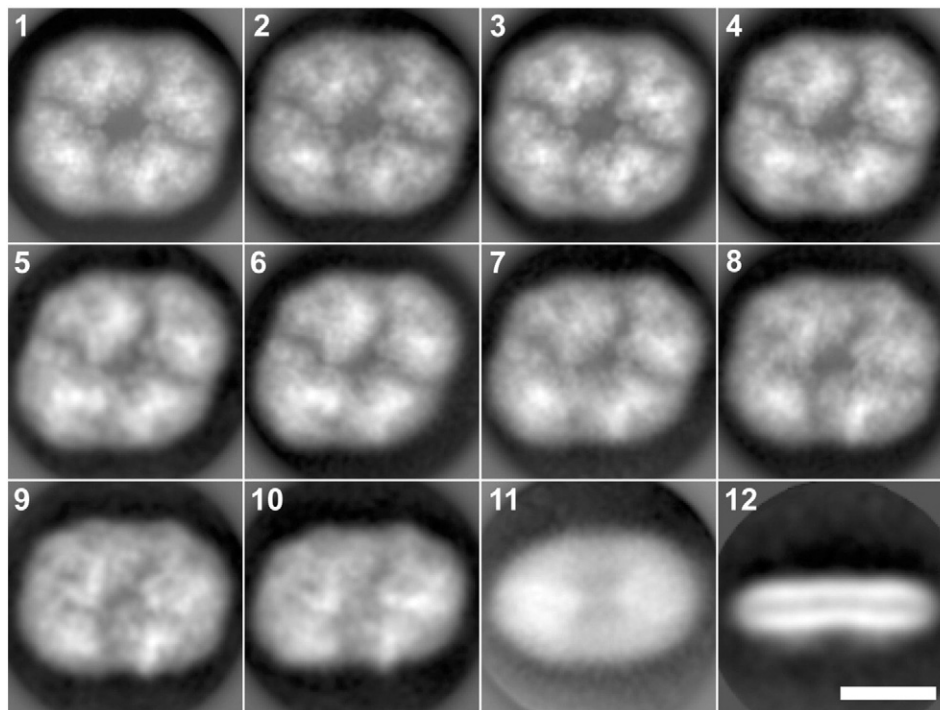


**Fig. 1.** 2D class averages of PSI tetramer projections from TS-821. Some classes represent top-views, with PSI seen as in the membrane plane (1–3), some others show the complex in side-view position (12), whereas others represent particles in views intermediate between top- and side-views (in particular frame 11). Numbers of summed particles are 34,000–45,000 for classes 1–4; 17,000–25,000 for classes 5–10; 9000 for 11 and 3000 for 12. Scale bar is 100 Å.

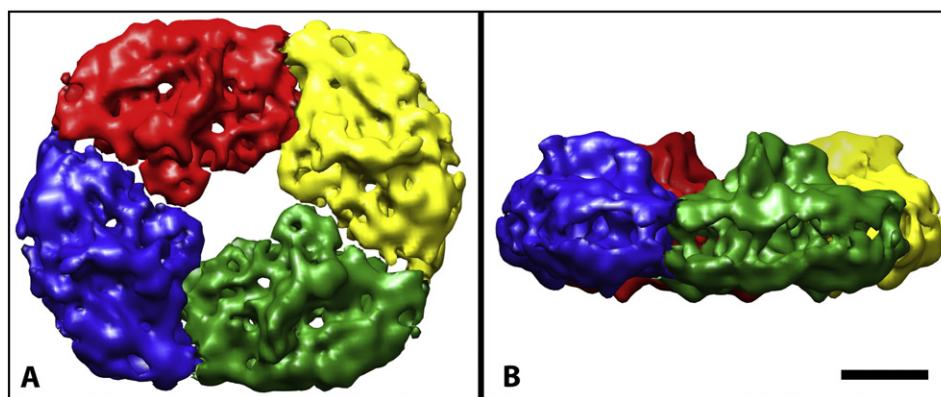


**Fig. 2.** The 11.5 Å structure of TS-821 tetrameric PSI from TS-821 with each of the 4 monomers in a different color. A - The PSI tetramer, as seen from the stromal side of the membrane. The tetramer is comprised of two equal dimers: red-blue and green-yellow. B - View of the tetramer parallel to the membrane plane. Scale bar is 50 Å.

condition, the culture was maintained in a 2 l bottle with aeration at 0.5 VVM of filtered air in a growth incubator. However, to obtain the high light conditions (HL, 800  $\mu\text{E}/\text{m}^2/\text{s}$ ) growth was carried out in a flat plate airlift 25 l photobioreactor (Photon Systems Instruments, Czech Republic) with LED illumination. Both cultures were maintained at 45 °C. To analyze the PSI oligomer ratio shift, isolated thylakoids from those cells were solubilized in varying concentration of  $\beta$ -DDM with final Chl concentration at 0.2 mg/ml and analyzed using BN-PAGE as described before [1,22]. A parallel analysis was done using 10–30% sucrose density gradient centrifugation by loading solubilized thylakoids (0.4 mg/ml Chl in 0.6%  $\beta$ -DDM). The result is shown in Fig. 8B after spinning at 30,000 rpm (SW32 Ti rotor, Beckman) for 24 h.

### 2.3. Cryo-electron microscopy

Quantifoil holey carbon supported grids R 3.5/1 200 mesh were covered manually with a thin layer of carbon prepared using a carbon evaporator (Edwards). For cryo-EM samples containing ~0.02 mg PSI/ml. Quantifoil grids were glow-discharged before sample application. For plunge-freezing a FEI Vitrobot was used. The adsorption time of the sample on the Quantifoil carbon coated grid was 1 min. Cryo-EM was performed on a FEI G2 Polara microscope operated at 300 kV, with a Gatan energy filter in zero-loss mode with a total dose approximately 25  $\text{e}^-/\text{Å}^2$ . Micrographs were recorded with a Gatan 2k  $\times$  2k CCD camera at 115,000 $\times$  magnification at the camera level, corresponding with a pixel size at the specimen level of 2.63 Å. Micrographs were collected

in series with defocus values of 3.5  $\mu\text{m}$ , 3  $\mu\text{m}$ , 2.5  $\mu\text{m}$  and 2  $\mu\text{m}$ . GRACE software was used for semi-automated data acquisition [23].

### 2.4. Data processing

Image analysis was performed on a cluster with 8 nodes (16 cores per node, Intel(R) Xeon(R) CPU E5-2650 v2 @ 2.60 GHz) and 64 GB memory per node. In total, 9005 micrographs were used for extracting 338,027 single-particle projections. Image analysis was done using both XMIPP and RELION-1.3 [24] software. 3D refinement of the obtained structure was done using the “gold standard” method in RELION-1.3 [24].

### 2.5. Molecular fitting and analysis

Fitting was done using UCSF Chimera software [25]. For fitting purposes, the high-resolution crystal structure of Photosystem I from *T. elongatus* (PDB entry: 1JB0) was used. The PsaL subunit of *Chroococcidiopsis* was modeled using its known protein sequence (UniProtKB entry: V5JYE0) on the SWISS-MODEL [26] website. As a template the 4xk8.1.L crystal structure of plant photosystem I-LHCI super-complex at 2.8 Å resolution was used. The template has 47.55% identity to the modeling structure. The obtained PsaL subunit from *Chroococcidiopsis* substituted the original PsaL of *T. elongatus* in 1JB0 crystal structure using UCSF Chimera [25]. The amino acid sequence alignment of different PsaL subunits of PSI and investigation for

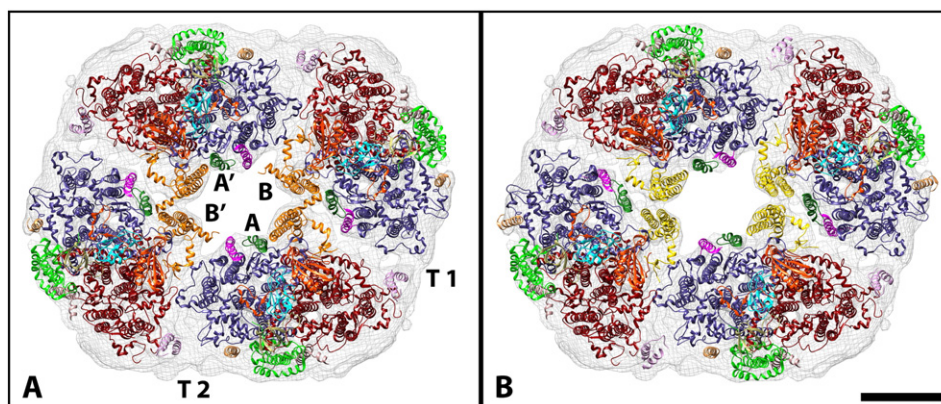


**Fig. 3.** 3D model of the TS-821 tetramer with the atomic structure of PSI from *T. elongatus* fitted in. A - Model with the crystal structure of *T. elongatus* fitted as a rigid body inside the 3D volume map of TS-821, shown as a mesh. B - Model with the subunits of the crystal structure of *T. elongatus* fitted separately into the 3D volume. The PsaL subunit is the modeled structure for TS-821 based on the a.a. sequence and PsaL from *P. sativum* as a template. The four monomers inside the TS-821 tetramer are named A, B, A', B' and the two interface types between monomers T 1 and T 2. The models show a view from the stromal side. Pigments have been omitted. 3D volume map is shown as a mesh. Colors of the subunits: PsaA - dark red; PsaB - dark slate blue; PsaD - orange red; PsaL (original) - orange; PsaL (modeled) - gold; PsaI - forest green; PsaM - magenta; PsaK - plumb; PsaX - sandy brown. Scale bar is 50 Å.

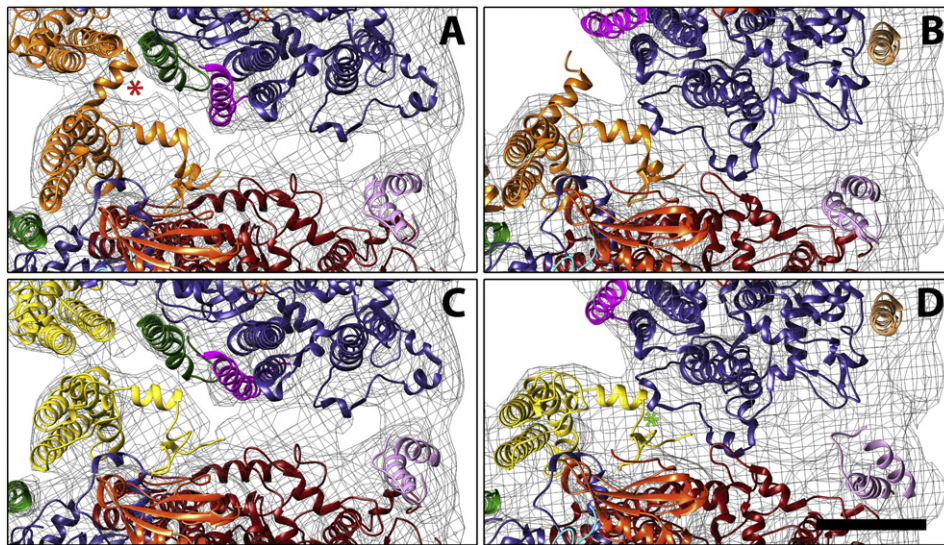


**Fig. 4.** Comparison of TS-821 inter-monomer spaces. A - Interface type 1 with the crystal structure of *T. elongatus* fitted as a rigid body into the 3D volume map of TS-821. B - Interface type 2 with the crystal structure of *T. elongatus* fitted as a rigid body. C - Interface type 1 with the crystal structure of *T. elongatus* fitted into the 3D volume map of TS-821. The subunits were fitted separately and PsaL is substituted by the modeled one from TS-821. D - Same as in C for interface type 2. Colors of the subunits as in Fig. 3. Scale bar is 50 Å.

presence of contacts between different subunits in the intermonomer space was made by UCSF Chimera [25].

### 3. Results

To obtain structural insight into the *Chroococcidiopsis* PSI tetramer we used a large cryo-EM data set, which was first classified using RELION applying standard procedures and routines, including phase contrast transfer correction and particle alignments. The 12 most populated classes show 2D maps of intact tetramers in different orientations, including top-views and side-views (Fig. 1). Collectively, these 12 classes contained about 47% of the initial data set and were used for getting an initial 3D model. The remaining 53% of the particles were either poorly focused, aggregated or in some other way low-quality and were discarded. In a next step, 3D classification was performed for which an initial reference with imposed C2 symmetry was used. As a result, twenty 3D classes were obtained that in total included 157,845 particles. Among them one 3D class, which had the highest resolution, included 23,145 particles. This most consistent 3D class was further refined and post-processed with B-factor sharpening. The resulting 3D structure had an overall resolution of 11.5 Å by the “gold standard” Fourier shell correlation (FSC) = 0.143 criterion (Fig. 2). The best non-symmetrized 2D map of the tetramer, almost in

the plane of the membrane, showed ~6.1 Å resolution and included 45,901 particles (Fig. 1).

The obtained 3D volume confirms that photosystem I from TS-821 is a tetramer with C2 type of symmetry (Fig. 2). It means that the tetramer is a dimer of dimers (red-blue and green-yellow, resp.) and that the monomer can take two different non-equivalent positions (A and B in Fig. 3) in the assembly. Neighboring monomers are related by a rotation of 114° and 66°, respectively, resulting in two different monomer interfaces, annotated as type 1 and type 2 (Fig. 3). To get further insight into the orientation and interaction of the monomers in the tetrameric PSI complex from TS-821, the crystal structure of the *T. elongatus* monomer (PDB entry: 1JB0) was fitted into the 3D density, initially as a rigid body. The overall fit suggests that there is no major rearrangement of the subunits comprising the monomer. The main discrepancy was an absence of density for the PsaL subunit in the C-terminal region (Fig. 4A, B, region marked with a red asterisk). Therefore, it was decided to try to model PsaL based on the known primary structure and homology with the pea *Pisum sativum* PsaL structure, and subsequently fit all individual subunits into the TS-821 3D density.

The primary structure alignment of PsaL subunit from TS-821, *P. sativum* and *T. elongatus* showed an absence of 9 amino acids in the *T. elongatus* PsaL subunit sequence at position 112–123. This place is filled by VATVTPNP in TS-821 and APSLTLGRKKE in *P. sativum* and

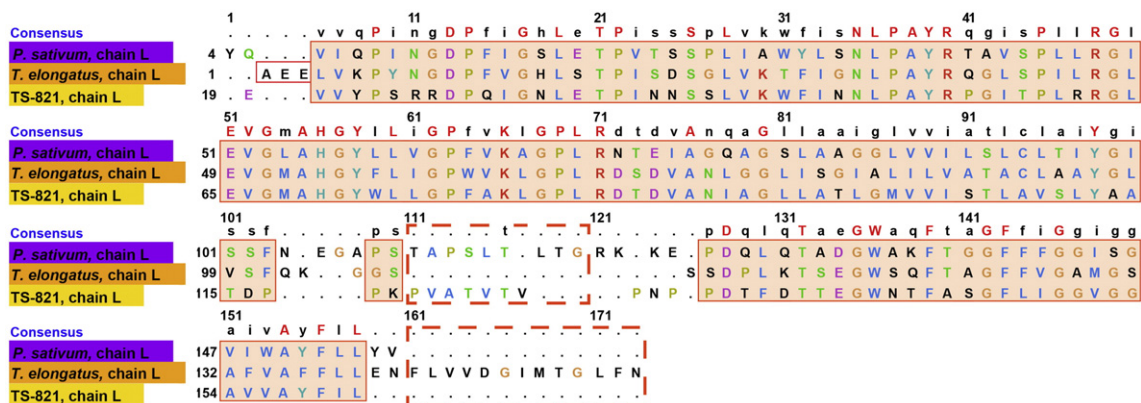


**Fig. 5.** Aligned amino acid sequences of PsaL subunits from three different species. Consensus bar shows consensus in the presence of the conserved residues, if capitalized and shown in red – the residues are the completely conserved (for three comparable species). The upper dashed red rectangular frame focused on the area with extra amino acid sequence presence in *P. sativum* and TS-821. The lower one – on the long C-terminus of *T. elongatus*.

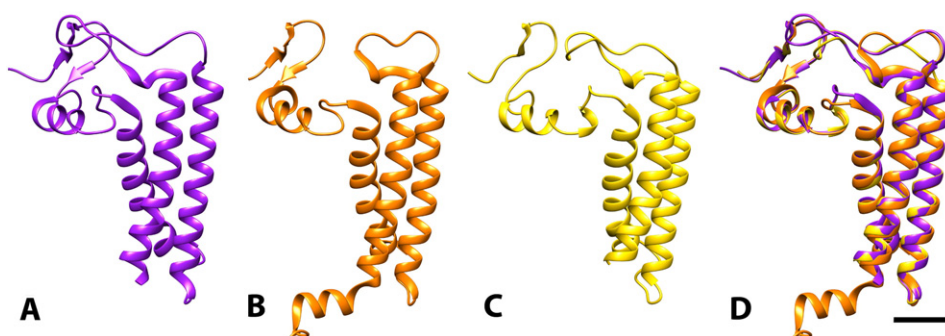


**Fig. 6.** Ribbon view of secondary structure of PsaL subunits from some photosystems I. A - PsaL subunit from PS I of *P. sativum* (PDB entry: 4xk8.1.L). B - PsaL subunit from PS I of *T. elongatus* (PDB entry: 1JB0). C - PsaL subunit from PS I of TS-821, modeled based on PDB entry: 4xk8. D - Overlapped PsaL subunits structures of A–C. The view is along the membrane plane. Top of each ribbon – n-side (stromal), bottom – p-side (luminal). Scale bar is 25 Å.

located on the stromal side of the PSI monomer (Fig. 5). Also there is a difference in length of C-termini of PsaL from these species: *T. elongatus* has the longest C-terminus, whereas the C-terminus of PsaL of *P. sativum* and TS-821 are shorter and comparable in length (Fig. 5).

Based on the known amino acid sequence [1], the PsaL subunit of TS-821 was modeled using PsaL subunit of *P. sativum* as a template (PDB entry: 4Y28.L) (Fig. 6). The modeled PsaL subunit of TS-821 was used to substitute the existing PsaL subunit in crystal structure of *T. elongatus* (Fig. 3B) and most of the subunits from the crystal structure of *T. elongatus* were fitted separately into the 3D volume map of TS-821 (Figs. 3B and 4C, D). The densities for PsaX in monomer A and PsaC and PsaF in monomer B were not sufficiently well defined to allow individual subunit fitting. They were placed based on the rigid body PSI monomer fit.

The modeled PsaL fits much better in the experimental 3D density than the homologous *T. elongatus* structure (Fig. 4). The main difference is in the C-terminal PsaL-h helix in *T. elongatus* (marked with an asterisk in Fig. 4A, B), which is absent in TS-821. A consequence of the 2-fold rotational symmetry in the TS-821 PSI tetramer is the presence of 2 different types of interfaces between the monomers: type 1 between monomers A and B, and type 2 between monomers A and B' (Fig. 3). Fig. 4 shows a closer look at the two interfaces for both the *T. elongatus* crystal structure fitted as a rigid body and the *T. elongatus* crystal structure with substituted TS-821 PsaL subunit and with each subunit fitted separately.

The type 1 interface for the rigid body fitted structure revealed contacts between subunits PsaL–PsaB, PsaL–PsaL, PsaL–PsaA, PsaA–PsaB, and PsaA–PsaM. After replacing PsaL with the TS-821 modeled version and fitting all subunits individually only contacts between subunits PsaL–PsaL, PsaL–PsaA, PsaA–PsaB, and PsaA–PsaM were apparent. However, in the type 2 interface shown (after fitting the crystal structure as a rigid body) revealed only contacts between subunits PsaA and PsaB. However using the modeled PsaL and after

additional individual fitting, an additional contact between PsaL and PsaB was observed, shown in Fig. 4D with a green asterisks.

The type 1 interface in TS-821 is similar to the monomer interface in the trimeric PSI from *T. elongatus*, in which all monomers are related by a 120° rotation (Fig. 7) instead of 114°. The main difference is near the center of the complex, where PsaL in *T. elongatus* makes contact with subunits PsaA, PsaB, and PsaM in the neighboring subunit, in addition to the contacts found in the TS-821 model. The more extended contacts near the center in *T. elongatus* PSI is a consequence of the different relative monomer orientation and also of the  $\alpha$ -helical extension at the C-terminus of the subunit, which penetrates into the neighboring monomer. This results in the formation of a significant cavity in the central part of the tetramer. This cavity occupies nearly 1800 Å<sup>2</sup> of surface area, yet it is not clear if this is filled with lipids or some other lipophilic molecules like carotenoids.

To explore the physiological role PSI tetramer plays, the multimeric state was investigated under two different growth conditions: low light (LL, 40  $\mu\text{E}/\text{m}^2/\text{s}$ ) and high light (HL, 800  $\mu\text{E}/\text{m}^2/\text{s}$ ). The oligomeric profiles under different light intensities were examined by BN-PAGE analysis after thylakoid membrane solubilization with variable  $\beta$ -DDM concentrations (Fig. 8A). Under both conditions, PSI monomer, dimer, and tetramer are dominant oligomeric states compared with a less abundant trimeric PSI species. However, under LL, the amount of PSI trimer is higher than that under HL (Fig. 8A). This is more easily observed after staining with CBB (Fig. 8B). In contrast, cells grown under high light contain a much higher amount of the PSI tetramer (Fig. 8A, B). This difference can also be distinguished without BN-PAGE since the increase in the amount of chlorophyll migrating as a tetramer is easily observed using sucrose density gradient centrifugation (Fig. 8C). This figure also shows an obvious increase of the trimer under low light conditions as is clear from the new chlorophyll containing band. At the same time, it seems that under the same detergent concentration, dimeric PSI is less abundant under HL compared to those under LL. PSI tetramer can dissociate into dimers and monomers upon detergent

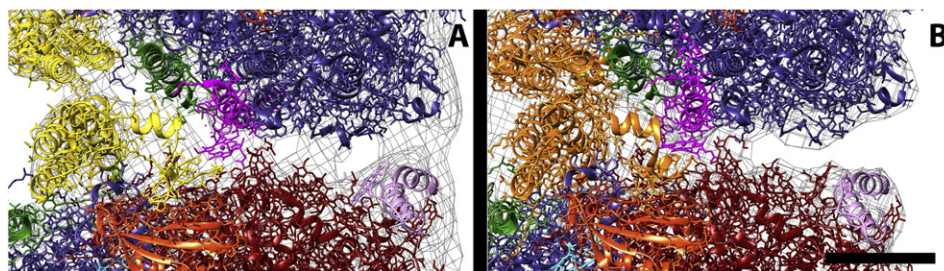


**Fig. 7.** Comparison of trimeric interface of *T. elongatus* with interface type 1 of TS-821. A - Interface type 1 with the crystal structure of *T. elongatus* fitted into the 3D volume map of TS-821 where the subunits were fitted individually and PsaL subunit is substituted by the modeled one from TS-821. All atoms and bonds, including those from the pigments, are shown. B - Interface of the trimeric PSI crystal structure fitted into the same 3D volume density map of *T. elongatus* at 11.5 Å. Subunits colored the same as on previous figures. Scale bar is 50 Å.

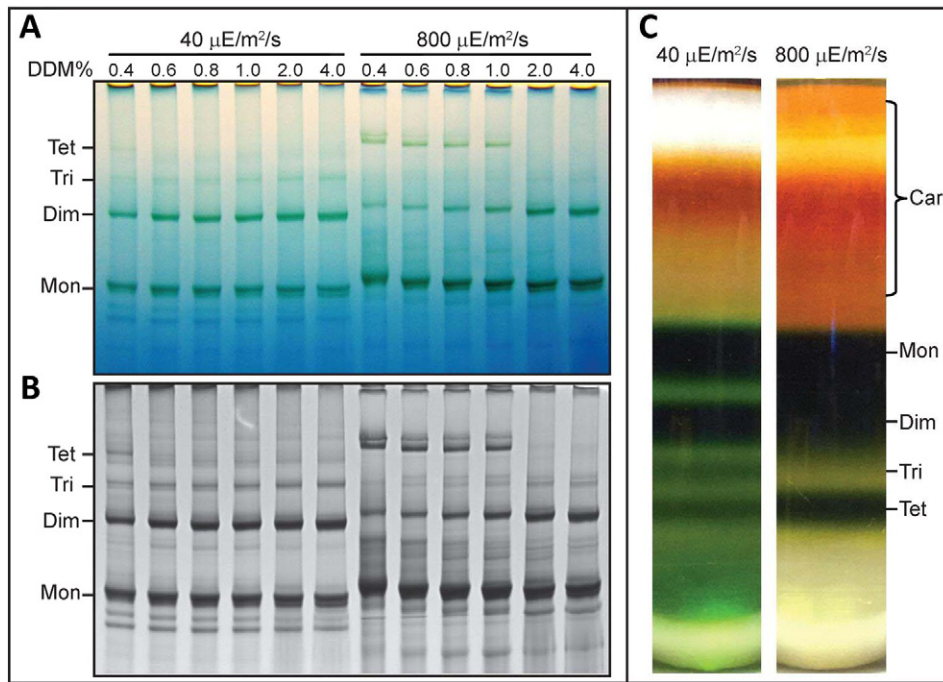


**Fig. 8.** Comparison of *Chroococcidiopsis* PSI oligomeric profiles under different light intensities. A - The unstained BN-PAGE analysis of TS-821 thylakoid membranes solubilized with the indicated % of DDM. The left lanes are the low light (40  $\mu\text{E}/\text{m}^2/\text{s}$ ) and the right lanes are the high light (800  $\mu\text{E}/\text{m}^2/\text{s}$ ). B - This is the same BN-PAGE gel following staining with CBB to enhance clarity. C - Sucrose density gradient centrifugation of solubilized TS-821 thylakoid membrane isolated from cells grown under different light conditions. Main bands corresponding to carotenoids (Car), PSI monomer (Mon), dimer (Dim), trimer (Tri), and tetramer (Tet) are labeled.

treatment [1]. Another noticeable difference between LL and HL is that PSI tetramer is more stable under HL, judging by its resistance to higher detergent ( $\beta$ -DDM) concentration (Fig. 8A). Besides more PSI tetramer and less trimer under HL, more carotenoids can also be found under HL condition in the sucrose density gradient after centrifugation (Fig. 8C).

Under LL, there are also traces of other bands that become better visible after Coomassie staining (Fig. 8B). Single particle electron

microscopy plus classification was performed on negatively stained specimens of the initially purified tetramer to reveal additional types of multimers (Fig. 9). Analysis showed the expected tetramers (Fig. 9A, B) and dimers (Fig. 9D). Although classical negative stain was used, some classes show a very detailed map (Fig. 9A). Although these were purified as tetramers, we also observed small numbers of trimers (Fig. 9E). Further, some tetramers and trimers appear to have an extra dimer associated (Fig. 9C, F). The extra trimer is only loosely bound to

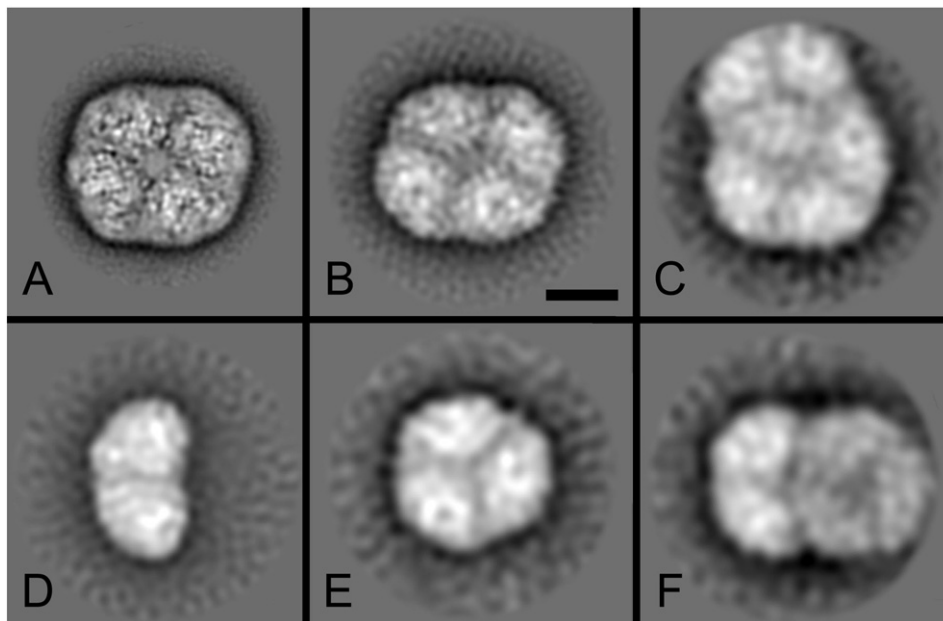


**Fig. 9.** Analysis of multimers of TS-821 by single particle electron microscopy. A - Best tetramer 2D projection map from 3700 summed particles at 8.1 Å resolution in negative stain from a homogeneous preparation of tetramers. B - Tetramer map out of an analyzed data set of all possible multimers. C - tetramer with a dimer attached at the top. D - dimer map. E - trimer map. F - trimer with a dimer attached at the left. The amount of detail visible in frames B–F reflects about the number of projections summed for each type of 2D map. Number of particles for frames B–F was 1043, 519, 892, 657 and 487, respectively. Scale bar is 100 Å.

the tetramer, as the band disappears in gels at detergent concentrations above 0.4% DDM. It is not known if these are functionally active multimers or reflect some type of aggregation. The fact that only traces are present suggests that these complexes are likely irrelevant for the overall light-harvesting and PSI function.

#### 4. Discussion

Our results confirm that the PSI supercomplex of TS-821 has a tetrameric organization with C2 symmetry. The absence of 4-fold rotational symmetry leads to two different, non-equivalent, monomer positions in the tetramer and to the existence of two different monomer interfaces. One interface (type 1) is similar to that in trimeric PSI from *T. elongatus*. The second interface is quite different in the contacts between subunits. In preparations of TS-821 PSI, dimers have been observed in addition to the tetramers (Fig. 9). These dimers were exclusively built from monomers (A and B, Fig. 3A) connected by a type I interface. This suggests that the type 1 interaction is stronger than the type 2, and that the tetramer can be considered a dimer of (A–B) dimers.

To get more insight into the binding interactions in the two interfaces, a homologous high-resolution X-ray structure of PSI from *T. elongatus* was fitted into our density map for TS-821. Initially as a rigid body fit at the monomer level, but the position and orientation of most subunits could be refined individually. Interactions could be described at the level of secondary structure elements. The current resolution of 11.5 Å is not sufficient to draw more detailed conclusions about interactions at the amino acid level and the location of pigments that play an important role in the transfer of energy.

Because the PsaL subunit from the crystal structure of *T. elongatus* did not fit well inside the experimentally obtained 3D density map, the PsaL from TS-821 was modeled based on the amino acid sequence using the *P. sativum* crystal structure as a template. This gave a much better fit, but also shows the less close interaction between PsaL subunits from neighboring monomers due to the absence of the C-terminal L-h helix from *T. elongatus*. PsaL plays a central role in the trimer formation of *T. elongatus* PSI [2]. The absence of the C-terminal L-h helix in TS-821 may explain the formation of tetramers, because of a weaker binding between L subunits over the type 1 interface, allowing for a second type of interaction via the type 2 interface.

Currently it is not understood what the potential advantage for *Chroococcidiopsis* is in forming tetrameric PSI rather than solely trimeric complexes as in *T. elongatus*. In *T. elongatus* there is a dynamic equilibrium between monomers and trimers, but under normal physiological conditions the equilibrium is by far on the side of the trimers [27]. One option for *Chroococcidiopsis* is that there is a dynamic equilibrium between monomers, dimers and tetramers, which opens the possibility to respond to changes in light level. As shown in Fig. 8, in response to changes in light levels TS-821 seems to change the ratio of PSI dimers to monomers plus tetramers. The tetramers are clearly more abundant under HL conditions while the amount of trimer increases under LL. Considering the presence of two copies of *psaL* genes in some cyanobacteria such as *Chroococcidiopsis thermalis* PCC 7203 [1], it is relevant to consider if TS-821 may have two *psaL* genes that are alternatively expressed under different light conditions. We have recently sequenced TS-821 genome with over 36 million MiSeq desktop sequencer reads of 300 bp. This has allowed us to assemble and annotate a draft genome by shotgun sequencing (unpublished results). Analysis of this genome shows no presence of a second copy of *psaL* gene was found in TS-821. We now speculate that TS-821 only has one form of PsaL in all oligomeric forms of PSI. This means that the difference in PSI tetramer and PSI trimer may result from other changes that could include changes in lipid composition, fatty acid profile, carotenoids or may involve an unknown subunit in the complex. However, our ongoing proteomic data does not support this latter explanation. At this moment, we are not sure if other proteins are involved in stabilizing the tetramer. We do not rule out the possibility, but currently favor

the modulation by the carotenoids, since we have also observed a change in the carotenoid content in the thylakoid membrane under high light growth conditions (Fig. 8B).

Analysis of negatively stained TS-821 trimeric particles (Fig. 9E) indicates that their overall structure resembles the one of *T. elongatus*. The trimeric PSI of *T. elongatus* has been shown to have cooperativity among monomers [28,29], which suggests that trimeric PSI is an adaptation to low light intensity. The fact that trimeric PSI is more abundant under LL (Fig. 8) does support the hypothesis. In contrast, the tetrameric PSI is more stable and dominant under HL (Fig. 8), indicating that tetrameric PSI is more resistant to high light intensity. As mentioned above, the observed elevated content of carotenoids (Fig. 8B) may explain why tetrameric PSI is more suitable under HL conditions. At the same time, carotenoids may be a stabilization cofactor for the tetrameric PSI or could even be accumulating within the central cavity of the tetramer. Other possibilities may include a more efficient or rapid interaction with phycobilisomes during state transitions as has been suggested by the prior identification of a bound PBS rod to the tetrameric form [20,21]. A higher resolution structure is required to explore this further and to understand the tetramer formation and energy transfer in more detail.

A more general question concerns the distribution of tetramer-forming PSI species within the phylum of cyanobacteria. The species of this study, *Chroococcidiopsis* sp. TS-821, is a member of the unicellular subsection II. The other PSI tetramer studied in detail is from *Anabaena* sp. PCC 7120 [21], a heterocyst-forming cyanobacterium from the filamentous subsection IV. The fact that both species were not originally thought to be closely related suggests a wide distribution of the tetrameric PSI association, making further study to this particular PSI of interest. It will be interesting to investigate a more wide range of cyanobacteria to determine just how widespread this tetrameric form of PSI is in cyanobacteria.

#### Acknowledgments

Support has been provided from the Gibson Family Foundation, the Bredesen Center for Interdisciplinary Research and Education, the Tennessee Plant Research Center, a UTK Professional Development Award, and National Science Foundation support to B.D.B. (DGE-0801470 and EPS-1004083). M.L. has been supported as a CIRE Fellow at University of Tennessee, Knoxville. Travel of B.D.B. to The Netherlands was supported by a Professional Development Award from the Graduate School at UTK. Work at University of Groningen was supported by NWO Chemical Sciences.

#### References

- [1] M. Li, D.A. Semchonok, E.J. Boekema, B.D. Bruce, Characterization and evolution of tetrameric photosystem I from the thermophilic cyanobacterium *Chroococcidiopsis* sp. TS-821, *Plant Cell* 26 (2014) 1230–1245, <http://dx.doi.org/10.1105/tpc.113.120782>.
- [2] I. Grothjohann, P. Fromme, Structure of cyanobacterial photosystem I, *Photosynth. Res.* 85 (2005) 51–72, <http://dx.doi.org/10.1007/s11120-005-1440-4>.
- [3] P. Jordan, P. Fromme, H.T. Witt, O. Klukas, W. Saenger, N. Krauss, Three-dimensional structure of cyanobacterial photosystem I at 2.5 Å resolution, *Nature* 411 (2001) 909–917, <http://dx.doi.org/10.1038/35082000>.
- [4] A. Ben-Shem, F. Frolow, N. Nelson, Crystal structure of plant photosystem I, *Nature* 426 (2003) 630–635, <http://dx.doi.org/10.1038/nature02200>.
- [5] A. Amunts, O. Drory, N. Nelson, The structure of a plant photosystem I supercomplex at 3.4 Å resolution, *Nature* 447 (2007) 58–63, <http://dx.doi.org/10.1038/nature05687>.
- [6] N. Krauss, W.D. Schubert, O. Klukas, P. Fromme, H.T. Witt, W. Saenger, Photosystem I at 4 Å resolution represents the first structural model of a joint photosynthetic reaction centre and core antenna system, *Nat. Struct. Biol.* 3 (1996) 965–973, <http://dx.doi.org/10.1038/nsb1196-965>.
- [7] P. Fromme, P. Jordan, N. Krauß, Structure of photosystem I, *Biochim. Biophys. Acta Bioenerg.* 1507 (2001) 5–31, [http://dx.doi.org/10.1016/S0005-2728\(01\)00195-5](http://dx.doi.org/10.1016/S0005-2728(01)00195-5).
- [8] E. El-Mohsnawy, M.J. Kopiczak, E. Schlodder, M. Nowaczyk, H.E. Meyer, B. Warscheid, et al., Structure and function of intact photosystem I monomers from the cyanobacterium *Thermosynechococcus elongatus*, *Biochemistry* 49 (2010) 4740–4751, <http://dx.doi.org/10.1021/bi901807p>.

- [9] M.K. Sener, C. Jolley, A. Ben-Shem, P. Fromme, N. Nelson, R. Croce, et al., Comparison of the light-harvesting networks of plant and cyanobacterial photosystem I, *Biophys. J.* 89 (2005) 1630–1642, <http://dx.doi.org/10.1529/biophysj.105.066464>.
- [10] P. Fromme, I. Grotjohann, Structure of cyanobacterial photosystems I and II, in: G.A. Peschek, C. Obinger, G. Renger (Eds.), *Bioenergetic Processes of Cyanobacteria*, Springer, Netherlands, 2011 (doi:10.1007/978-94-007-0388-9).
- [11] J.A. Ihalainen, P.E. Jensen, A. Haldrup, I.H.M. van Stokkum, R. van Grondelle, H.V. Scheller, et al., Pigment organization and energy transfer dynamics in isolated photosystem I (PSI) complexes from *Arabidopsis thaliana* depleted of the PSI-G, PSI-K, PSI-L, or PSI-N subunit, *Biophys. J.* 83 (2002) 2190–2201, [http://dx.doi.org/10.1016/S0006-3495\(02\)73979-9](http://dx.doi.org/10.1016/S0006-3495(02)73979-9).
- [12] H.V. Scheller, P.E. Jensen, A. Haldrup, C. Lunde, J. Knoetzel, Role of subunits in eukaryotic photosystem I, *Biochim. Biophys. Acta* 1507 (2001) 41–60, [http://dx.doi.org/10.1016/S0005-2728\(01\)00196-7](http://dx.doi.org/10.1016/S0005-2728(01)00196-7).
- [13] J. Knoetzel, A. Mant, A. Haldrup, P.E. Jensen, H.V. Scheller, PSI-O, a new 10-kDa subunit of eukaryotic photosystem I, *FEBS Lett.* 510 (2002) 145–148, [http://dx.doi.org/10.1016/S0014-5793\(01\)03253-7](http://dx.doi.org/10.1016/S0014-5793(01)03253-7).
- [14] B. Drop, M. Webber-Birungi, F. Fusetti, R. Kouřil, R.K.E. Redding, E.J. Boekema, R. Croce, Photosystem I of *Chlamydomonas reinhardtii* contains nine light-harvesting complexes (Lhca) located on one side of the core, *J. Biol. Chem.* 286 (2011) 44878–44887, <http://dx.doi.org/10.1074/jbc.M111.301101>.
- [15] C. Lunde, P.E. Jensen, A. Haldrup, J. Knoetzel, H.V. Scheller, The PSI-H subunit of photosystem I is essential for state transitions in plant photosynthesis, *Nature* 408 (2000) 613–615, <http://dx.doi.org/10.1038/35046121>.
- [16] E.J. Boekema, J.P. Dekker, M.G. van Heel, M. Rögner, W. Saenger, I. Witt, et al., Evidence for a trimeric organization of the photosystem I complex from the thermophilic cyanobacterium *Synechococcus* sp, *FEBS Lett.* 217 (1987) 283–286, [http://dx.doi.org/10.1016/0014-5793\(87\)80679-8](http://dx.doi.org/10.1016/0014-5793(87)80679-8).
- [17] E.J. Boekema, A. Hifney, A.E. Yakushevskaya, M. Piotrowski, W. Keegstra, S. Berry, et al., A giant chlorophyll-protein complex induced by iron deficiency in cyanobacteria, *Nature* 412 (2001) 745–748, <http://dx.doi.org/10.1038/35089104>.
- [18] O. Almog, G. Shoham, D. Michaeli, R. Nechushtai, Monomeric and trimeric forms of photosystem I reaction center of *Mastigocladus laminosus*: crystallization and preliminary characterization, *Proc. Natl. Acad. Sci. U. S. A.* 88 (1991) 5312–5316, <http://dx.doi.org/10.1073/pnas.88.12.5312>.
- [19] M. Brecht, M. Hussels, E. Schlodder, N.V. Karapetyan, Red antenna states of photosystem I trimers from *Arthrospira platensis* revealed by single-molecule spectroscopy, *Biochim. Biophys. Acta Bioenerg.* 1817 (2012) 445–452, <http://dx.doi.org/10.1016/j.bbabi.2011.11.012>.
- [20] M. Watanabe, H. Kubota, H. Wada, R. Narikawa, M. Ikeuchi, Novel supercomplex organization of photosystem I in *Anabaena* and *Cyanophora paradoxa*, *Plant Cell Physiol.* 52 (2011) 162–168, <http://dx.doi.org/10.1093/pcp/pcq183>.
- [21] M. Watanabe, D.A. Semchonok, M.T. Webber-Birungi, S. Ehira, K. Kondo, R. Narikawa, et al., Attachment of phycobilisomes in an antenna-photosystem I supercomplex of cyanobacteria, *Proc. Natl. Acad. Sci. U. S. A.* 111 (2014) 2512–2517, <http://dx.doi.org/10.1073/pnas.1320599111>.
- [22] I. Wittig, H.P. Braun, H. Schägger, Blue native PAGE, *Nat. Protoc.* 1 (2006) 418–428, <http://dx.doi.org/10.1002/pmic.201000343>.
- [23] G.T. Oostergetel, W. Keegstra, A. Brisson, Automation of specimen selection and data acquisition for protein electron crystallography, *Ultramicroscopy* 74 (1998) 47–59, [http://dx.doi.org/10.1016/S0304-3991\(98\)00022-9](http://dx.doi.org/10.1016/S0304-3991(98)00022-9).
- [24] S.H.W. Scheres, A bayesian view on cryo-EM structure determination, *J. Mol. Biol.* 415 (2012) 406–418, <http://dx.doi.org/10.1016/j.jmb.2011.11.010>.
- [25] E.F. Pettersen, T.D. Goddard, C.C. Huang, G.S. Couch, D.M. Greenblatt, E.C. Meng, et al., UCSF chimera — a visualization system for exploratory research and analysis, *J. Comput. Chem.* 25 (2004) 1605–1612, <http://dx.doi.org/10.1002/jcc.20084>.
- [26] M. Biasini, S. Bienert, A. Waterhouse, K. Arnold, G. Studer, T. Schmidt, et al., SWISS-MODEL: modelling protein tertiary and quaternary structure using evolutionary information, *Nucleic Acids Res.* 42 (2014), <http://dx.doi.org/10.1093/nar/gku340>.
- [27] E. El-Mohsnawy, M.J. Kopczak, E. Schlodder, M. Nowaczyk, H.E. Meyer, B. Warscheid, N.V. Karapetyan, M. Rögner, Structure and function of intact photosystem I monomers from the cyanobacterium *Thermosynechococcus elongatus*, *Biochemistry* 49 (2010) 4740–4751, <http://dx.doi.org/10.1021/bi901807p>.
- [28] D.R. Baker, A.K. Manocchi, M.L. Lamicq, M. Li, K. Nguyen, J.J. Sumner, B.D. Bruce, C.A. Lundgren, Comparative photoactivity and stability of isolated cyanobacterial monomeric and trimeric photosystem I, *J. Phys. Chem. B* 118 (2014) 2703–2711, <http://dx.doi.org/10.1021/jp407948p>.
- [29] I.J. Iwuchukwu, M. Vaughn, N. Myers, H. O'Neill, P. Frymier, B.D. Bruce, Self-organized photosynthetic nanoparticle for cell-free hydrogen production, *Nat. Nanotechnol.* 5 (2010) 73–79, <http://dx.doi.org/10.1038/nnano.2009.315>.